

PAPER

# Interfacial nanobubbles produced by long-time preserved cold water

To cite this article: Li-Min Zhou *et al* 2017 *Chinese Phys. B* **26** 106803

View the [article online](#) for updates and enhancements.

## Related content

- [Surface nanobubbles studied by atomic force microscopy techniques: Facts, fiction, and open questions](#)  
Holger Schönherr, Nicole Hain, Wiktoria Walczyk et al.
- [Nanobubbles and micropancakes: gaseous domains on immersed substrates](#)  
James R T Seddon and Detlef Lohse
- [Imaging surface nanobubbles at graphite–water interfaces with different atomic force microscopy modes](#)  
Chih-Wen Yang, Yi-Hsien Lu and Ing-Shouh Hwang

# Interfacial nanobubbles produced by long-time preserved cold water\*

Li-Min Zhou(周利民)<sup>1,4</sup>, Shuo Wang(王硕)<sup>1,4</sup>, Jie Qiu(邱杰)<sup>1,3,4</sup>, Lei Wang(王磊)<sup>1,2</sup>,  
Xing-Ya Wang(王兴亚)<sup>1,2,4</sup>, Bin Li(李宾)<sup>1,2</sup>, Li-Juan Zhang(张立娟)<sup>1,2,†</sup>, and Jun Hu(胡钧)<sup>1,2,‡</sup>

<sup>1</sup>Key Laboratory of Interfacial Physics and Technology, Shanghai Institute of Applied Physics, Chinese Academy of Sciences, Shanghai 201800, China

<sup>2</sup>Shanghai Synchrotron Radiation Facility, Shanghai Institute of Applied Physics, Chinese Academy of Sciences, Shanghai 201204, China

<sup>3</sup>School of Physical Science and Technology, Shanghai Tech University, Shanghai 201210, China

<sup>4</sup>University of Chinese Academy of Sciences, Beijing 100049, China

(Received 1 June 2017; revised manuscript received 25 July 2017; published online 10 September 2017)

Interfacial gaseous nanobubbles which have remarkable properties such as unexpectedly long lifetime and significant potential applications, are drawing more and more attention. However, the recent dispute about the contamination or gas inside the nanobubbles causes a large confusion due to the lack of simple and clean method to produce gas nanobubbles. Here we report a convenient and clean method to effectively produce interfacial nanobubbles based on a pure water system. By adding the cold water cooled at 4 °C for more than 48 h onto highly oriented pyrolytic graphite (HOPG) surface, we find that the average density and total volume of nanobubbles are increased to a high level and mainly dominated by the concentrations of the dissolved gases in cold water. Our findings and methods are crucial and helpful for settling the newly arisen debates on gas nanobubbles.

**Keywords:** nanobubbles, atomic force microscopy, gas saturation, solubility

**PACS:** 68.08.-p, 81.07.-b, 68.37.Ps, 64.75.Bc

**DOI:** 10.1088/1674-1056/26/10/106803

## 1. Introduction

Interfacial nanobubbles were first proposed to explain the steps of the force-separation curves while two hydrophobic solid surfaces were detached from each other in water in 1994.<sup>[1]</sup> Later, their existence was confirmed by directly observing the spherical cap-shaped structures on different substrates with atomic force microscopy (AFM) and other imaging tools.<sup>[2–7]</sup> Interfacial nanobubbles are thought to be involved in many processes such as boundary slip,<sup>[8,9]</sup> emulsion without surfactant,<sup>[10]</sup> microboiling,<sup>[11]</sup> rupture of a wetting film,<sup>[12]</sup> and may have potential applications in surface cleaning,<sup>[13,14]</sup> nanomaterial engineering,<sup>[15–17]</sup> and mineral floating.<sup>[18–20]</sup>

Although a large amount of the earlier research has been done, there are still some key questions needing to be further explored. The explanations of the large contact angle of nanobubble (from water side) and surprisingly long lifetime are the main issue.<sup>[21–29]</sup> Those properties could not be explained by traditional Epstein–Plesset theory based on Laplace law and diffusion equation, which predicts that bubbles on the order of nanometers will dissolve into water within microseconds.<sup>[30]</sup> Several theories like contamination layer,<sup>[31]</sup> dynamic-equilibrium,<sup>[23,27,32,33]</sup> and high density inside nanobubbles<sup>[34]</sup> have been proposed in order to solve

this puzzle. Nevertheless, the following research indicated that organic contaminant is not the cause of the stability and demonstrated that the gas inside the nanobubble is actually leaky.<sup>[35,36]</sup> The dynamic-equilibrium model was also criticized due to the lack of experimental evidence and the unclear driving mechanism of the gas influx near the contact line.<sup>[37,38]</sup> More recently, the contact-line pinning theory<sup>[29,39]</sup> proposed by Lohse and Zhang claimed that the local gas oversaturation and the pinning effects near the three-phase line were the reason for stabilizing the interfacial nanobubbles. Furthermore, the numerical calculation,<sup>[28]</sup> lattice density functional theory results<sup>[40]</sup> and molecular dynamics results<sup>[41,42]</sup> based on the pinning theory has successfully explained the large contact angle and the super-stability of a single nanobubble pinned on the heterogeneous surface. Despite the tremendous research progress of interfacial nanobubbles, many basic questions remain to be studied further. For example, we still do not know much about the properties of gas or water inside a nanobubble.<sup>[43]</sup> And disputes about the growth and mobility of nanobubbles and their effects on each other persist.<sup>[44–47]</sup> Except for interfacial nanobubbles, another gas state, micro-sized pancakes were often observed and could coexist with the interfacial nanobubbles.<sup>[48–52]</sup> Pancakes or gas enrichment layer underneath was also thought to stabilize

\*Project supported by the Key Laboratory of Interfacial Physics and Technology, Chinese Academy of Sciences, the Open Research Project of the Large Scientific Facility of the Chinese Academy of Sciences, the National Natural Science Foundation of China (Grant Nos. 11079050, 11290165, 11305252, 11575281, and U1532260), the National Key Basic Research Program of China (Grant Nos. 2012CB825705 and 2013CB932801), the National Natural Science Foundation for Outstanding Young Scientists, China (Grant No. 11225527), the Shanghai Academic Leadership Program, China (Grant No. 13XD1404400), and the Program of the Chinese Academy of Sciences (Grant Nos. KJCX2-EW-W09 and QYZDJ-SSW-SLH019).

†Corresponding author. E-mail: zhanglijuan@sinap.ac.cn

‡Corresponding author. E-mail: hujun@sinap.ac.cn

above nanobubbles.<sup>[47,53,54]</sup> Therefore, what is the relationship between nanobubbles and pancakes? Why are they stable at solid/water surfaces? Further researches are needed to address these significant issues.

The difficulties in answering those basic questions come from many aspects, and one of them is related to the production of clean gas-filled nanobubbles. A reliable and reproducible method of nanobubble formation is the primary task for nanobubble research. In order to produce nanobubbles on varied surfaces like mica, HOPG, gold, polystyrene, Octadecyltrichlorosilane (OTS) modified silicon and alumina surfaces, several methods were developed such as the solvent exchange process,<sup>[55,56]</sup> water–NaCl exchange process,<sup>[57]</sup> photo- and electrochemical methods.<sup>[58]</sup> Because of the difficulty in revealing the chemicals inside the nanobubbles based on current detecting methods, recently some scientists began to realize that some conflicting results obtained by those methods may be caused by the overlook of impurities involved in the experiments and the lack of control experiments to validate that the observed spherical cap-shaped objects were indeed gas-filled nanobubbles. Some reports pointed out that those spherical cap-shaped objects might be polydimethylsiloxane (PDMS) droplets instead of gas-filled nanobubbles due to the use of disposable needles in the exchange process.<sup>[38]</sup> Similarly, other researchers doubted the existence of gaseous micro-pancakes and claimed that these irregular micron-sized domains were merely polymeric layers due to the use of plastic syringes.<sup>[20]</sup> Therefore, there is an urgent requirement for a reliable, contamination-free and controllable method of producing the clean gas nanobubbles.

According to the current understanding, nanobubbles would be produced when the gas concentration in the solution is oversaturated in the process. In order to avoid being contaminated, it is better to produce nanobubbles by using pure water system. But the point is how to obtain the oversaturation state of gas in a pure water system. As is well known, gas is more soluble in water at lower temperature and less at high temperature. Thus, the gas will escape from the solution and achieve an oversaturated state when the temperature is increased. Previous report indicated that nanobubble could readily nucleate at a gas concentration of approximately 100%–110% and supersaturation was not a requirement.<sup>[25]</sup> According to this idea, recently researchers started to use pure water system to produce nanobubbles by changing the temperature and various methods were developed, such as temperature difference exchanging,<sup>[59]</sup> cold water deposited on hot substrate,<sup>[60]</sup> and microwave heating.<sup>[61]</sup> These methods were showed to be clean, but in order to achieve the high efficiency a high temperature or a high power was usually needed. However, high temperature or high power may seriously restrict the applications of nanobubbles in many important systems like

biology and medicine.

Here in this work, we develop a convenient one-step and controllable method to produce nanobubbles at HOPG/water surface by the gas-saturated cold water. In the whole process, the HOPG substrate is not treated by any heating process and only deionized pure water is used without any exchange process. The control experiments with degassing confirm that the nanobubbles produced by our method are indeed gaseous nanobubbles. The lateral sizes of the formed nanobubbles are about 100 nm–200 nm and distributed evenly on the HOPG substrate with a high efficiency of about 4~5 per  $\mu\text{m}^2$ . The gas concentration in cold water is found to be a key factor in forming the nanobubbles and the number of nanobubbles per  $\mu\text{m}^2$  could be controlled by cooling time.

## 2. Results and discussion

### 2.1. Characterization of nanobubbles

As shown in Fig. 1(a), when deionized water (25  $\mu\text{m}$ ) is directly added onto the HOPG surface, only bare graphite surface and steps could be seen in the height image. Nevertheless, when we add the cold water which is cooled at 4 °C for 72 h to the fresh HOPG surface and wait for more than twenty minutes at room temperature, a large number of spherical cap-shaped objects can be observed via PF-QNM imaging (Fig. 1(b)). The lateral dimensions of these spherical caps are around 100 nm–200 nm and the contact angles are above 150°. By performing PF-QNM imaging, we are able to acquire the stiffness information at the same time. The stiffness of those spherical cap-like objects is around 50 mN/m–150 mN/m (Fig. 2(a)) which is much softer than the substrate surface. Those results are consistent with the former observations about the morphology and stiffness of interfacial nanobubbles produced by water-ethanol exchange.<sup>[62]</sup> During the AFM scanning, we also find that most of the bubbles (size > 50 nm) are stable and hardly changed after scanning for several hours. In some cases, some smaller bubbles (size < 50 nm) disappear or newly form, which may be caused by the AFM tip during the scanning or the effects from the neighboring bubbles.

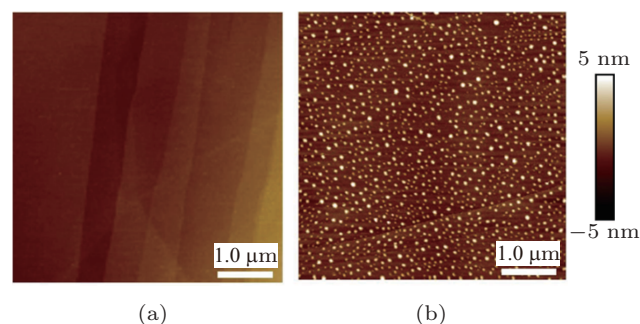


**Fig. 1.** (color online) AFM height images of HOPG surfaces using (a) room temperature water and (b) cold water after cooled at 4 °C for 72 h. The scan size is 5  $\mu\text{m}$   $\times$  5  $\mu\text{m}$ .

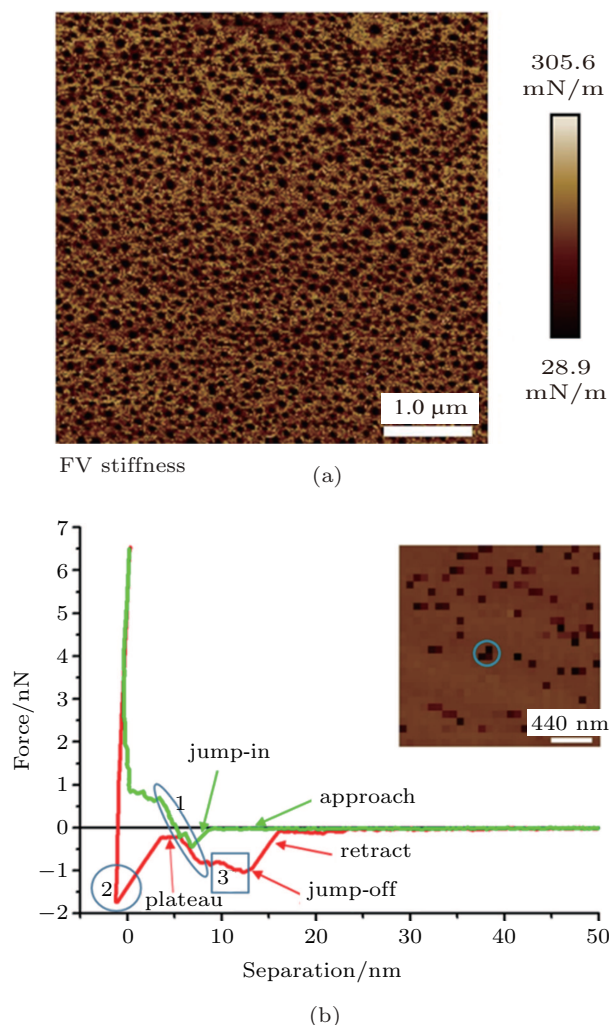


**Fig. 2.** (color online) (a) Stiffness image of nanobubbles in Fig. 1(b), and (b) force curves of a spherical cap-shaped object in force volume mode. The insert in panel (b) shows the slice (deflection error) image of the chosen nanobubble. Force curve is obtained on the nanobubble marked by blue circle. Panel (b) shows the three regions, i.e., region 1 (ellipse): linear-response region; region 2 (circle): retraction on substrate surface; region 3 (square): adhesion region.

The force curves of a spherical cap-shaped object acquired by force volume mode are shown in Fig. 2(b). In the experiment the calibrated spring constant of the silicon nitride tip is 0.3556 N/m and trigger threshold is set to 18.25 nm. As a result, the “trigger” peak force which leads to the retraction of the tip is about 6.5 nN. With such a large force, there is a very strong interaction between the tip and the substrate surface before retraction.

In the approaching curve (green line), the AFM tip firstly attached to the spherical cap-shaped object at about 10 nm, which is referred to as “jump-in” process. Then the AFM tip interacting with the object for about 8 nm in depth before reaching the HOPG surface. The tip-object interaction as shown in region 1 (ellipse) exhibits a quasi-linear response before touching the HOPG surface. The slope of the linear part is estimated at 1 nN/8 nm which is 125 mN/m. This is comparable to the surface tension of water 72 mN/m, which may indicate the gaseous property of the object. Those results

are consistent with the results reported previously, suggesting that the tip-bubble interaction is dominated by the repulsive force which increases linearly when the tip approaches to the bubble.<sup>[63–65]</sup> and agrees with simulation results of interaction between AFM tip and pinned nanobubble by using the lattice density functional theory.<sup>[66]</sup>

When retracting from the substrate surface as shown in the region 2 (circle), the AFM tip suffers a strong adhesion force ( $\sim 1.8$  nN). The reason for that may be that the tip has already “touched” the HOPG surface when such a large trigger force is reached. Note that the interaction between the tip and the object has a small plateau before the linear-response starts in region 1 (ellipse). The plateau has also been observed in several researches on force curves of nanobubble.<sup>[63,67]</sup> This phenomenon is not expected with a hydrophilic tip according to the dynamic interaction model. But it can be explained if the tip is hydrophobic and penetrated into the bubble near the substrate surface so that the contact line does not contribute to the interaction force.<sup>[63]</sup> Considering the fact that the AFM tip is plasma-cleaned to achieve hydrophilicity before the imaging process, neither a hydrophobic tip nor a contaminated tip cannot be the most possible reason for that plateau. A possible explanation may state as follows: the AFM tip which is not so hydrophilic is eventually penetrated into the object due to the large loading force (6.5 nN) while approaching to the substrate surface. Therefore, when the tip is withdrawn from the substrate surface, the contact line is not pinned on the AFM tip and slips several nanometers on the tip before being fully pinned on the tip. In such views, a small plateau then appears before the linear response of tip-object interaction. In the next step as shown in region 3 (square), the contact line still attaches to the “less hydrophilic” tip which leads to an attractive force until the tip is jumped off from the object surface. It is noted that most of the features are exhibited in Fig. 2(b) such as quasi-linear response, jump-in and adhesion force before jump-off, which are all consistent with the previous research results of the tip-nanobubble interaction<sup>[64,65]</sup> and also quite different from the forces curves of PDMS nanodroplets as reported recently.<sup>[67,68]</sup>

To further verify that those cap-shaped objects are indeed gaseous nanobubbles, we place the cold water into a vacuum chamber and degassed at a pressure lower than 10 mbar (1 bar =  $10^5$  Pa) for more than 2 hours. When the degassed cold water is injected into the HOPG surface and kept for more than 30 min before AFM imaging, only smooth graphite surface is observed as shown in Fig. 3(a). In the following experiment, we put the degassed water again into the refrigerator and cooled at 4 °C for another 72 h. When the re-cooled degassed water is added onto the HOPG surface and kept for about 30 min, the spherical cap-like objects appear on the substrate as shown in Fig. 3(b). In the degassing process, most of



the dissolved gases including  $N_2$  and  $O_2$  are removed from the water. Meanwhile the degassed water contacts only the ambient environment in the whole cooling process as described above, thus those spherical cap-shaped objects should be gas filled nanobubbles.

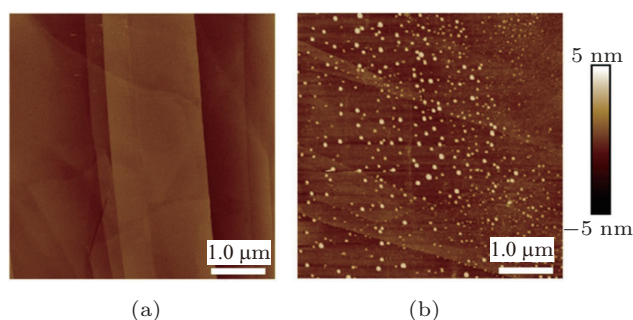


**Fig. 3.** (color online) The AFM height images of HOPG surfaces in (a) degassed water and (b) degassed water cooled for at 4 °C for 72 h. The scan size is 5  $\mu\text{m} \times 5 \mu\text{m}$ .

## 2.2. Controllable growth of nanobubbles

In order to find the appropriate experimental conditions for effective and controllable growth of nanobubbles, we further investigate the effects of different cooling time on the formation of interfacial nanobubbles. We cool the room temperature milipore water in the 4 °C refrigerator for 0 h, 2 h, 2 h, 2 h,

4 h, 6 h, 12 h, 24 h, 48 h, and 72 h, then deposited these cold water onto the HOPG surface. In Fig. 4, when adding the room temperature water onto the HOPG surface, nanobubbles are rarely formed. After adding the cold water with a certain cooling time (2 h, 4 h), some nanobubbles began to form on the substrate surface. More bubbles form on the graphite surface when the cold water is cooled for a longer time. Specifically, nanobubbles formed with longer cooling time (72 h, 48 h, 24 h) are slightly larger in size than those formed with shorter cooling times (12 h, 6 h, 4 h, 2 h). The number of nanobubbles per  $\mu\text{m}^2$  increases significantly with increasing cooling time. In addition, we find that the nanobubbles formed by our method are quite uniform in their lateral sizes (about 100 nm–200 nm) and distributed evenly on the HOPG surface as compared with those produced by water-ethanol exchange, where the lateral size and distribution of the nanobubbles vary a lot. This phenomenon may be attributed to the observation that the growth and stabilization of nanobubbles in our methods are much slower and moderate (about 30 min) while in other methods the environment near the HOPG surface is severely disturbed by the exchange process<sup>[69]</sup> or high substrate temperature.<sup>[60]</sup>

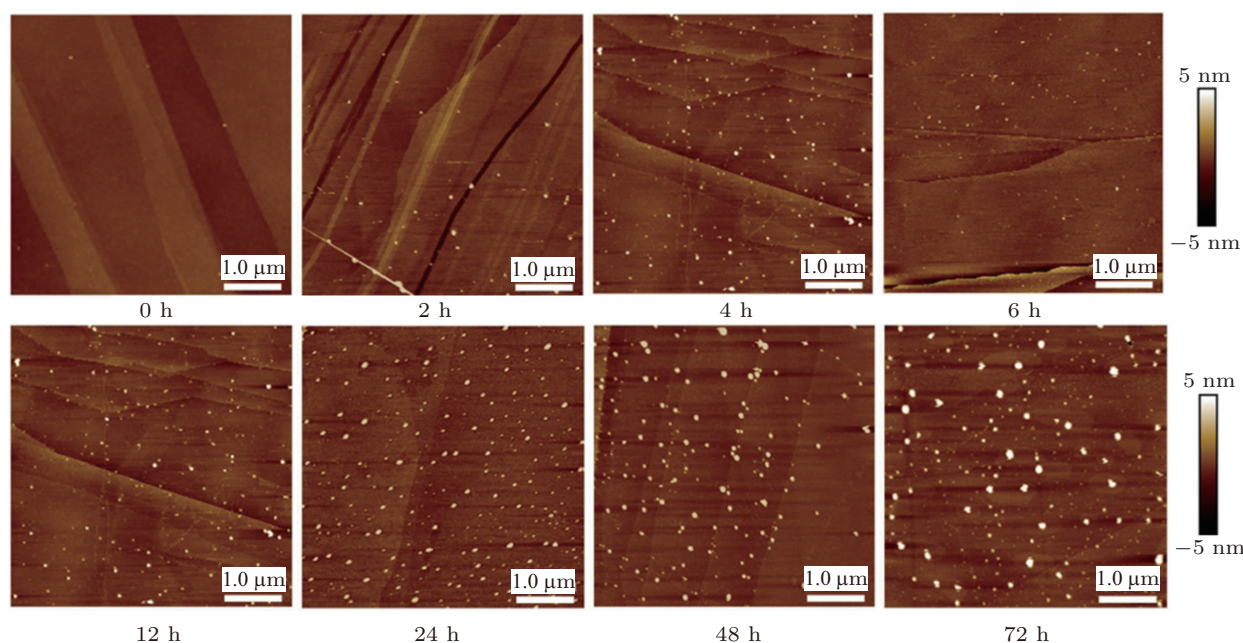


**Fig. 4.** (color online) The AFM images of interfacial nanobubbles formed by cold water after being cooled at 4 °C for 0 h, 2 h, 4 h, 6 h, 8 h, 12 h, 24 h, 48 h, and 72 h. The AFM image of 0 h is obtained by using room temperature water stored in ambient condition.

## 2.3. Quantitative analysis of density and volume of formed nanobubbles

The densities (number) and volumes of formed nanobubbles in water with different cooling times are analyzed to further explore the physical properties of nanobubbles. It has been generally recognized that the physical and chemical heterogeneities of substrate would affect the formation of the in-

terfacial nanobubbles. The nanobubbles formed on different substrates may be different even on the same substrate the nanobubbles are also different in different regions. For example, many nanobubbles tend to nucleate at the edge of the graphite steps as indicated by our observations. In order to reduce the substrate effects as much as possible and acquire a quantitative description about the nanobubbles formed by

cold water with different cooling times, we have the experiments repeated independently at least 5 times for each group, and select the different areas randomly for AFM imaging. After that, those AFM images are analyzed following the particle analysis procedure in the Nanoscope Analysis V1.5 software to count the numbers of nanobubbles and their average lateral size. We only count the nanobubbles with lateral dimension larger than 50 nm and height higher than 2 nm considering the larger error problem of small bubbles. In this process about 150 AFM height images with 13580 nanobubbles counted are analyzed in all the experiments for this work.

Since the nanobubbles formed by cooled water are all spherical cap-shaped and similar to each other in lateral size, we then calculate the density and total volume of the formed gaseous nanobubbles in the area from the following equations:

$$\bar{\rho} = \left\langle \frac{N}{25} \right\rangle. \quad (1)$$

$$\bar{V} = \left\langle \frac{\pi \bar{h}(3\bar{L}^2 + 4\bar{h}^2)N}{24} \right\rangle, \quad (2)$$

where  $N$  is the total number of nanobubbles in an AFM image,  $\bar{L}$  is the average Lateral size,  $\bar{h}$  is the average height,  $\bar{\rho}$  is the average density (number per  $\mu\text{m}^2$ ),  $\bar{V}$  is the average total volume of nanobubbles in the  $5\mu\text{m} \times 5\mu\text{m}$  area,  $\langle \rangle$  represents the average of each individual AFM image. The statistical data are shown in Fig. 5. A set of detailed data for nanobubbles produced by cold water cooled for 48 h at  $4^\circ\text{C}$  is provided in Table A1 in Appendix A.

In Fig. 5(a), the density of nanobubbles formed by degassed water indicates that long time cooling would greatly improve the efficiency of nanobubble formation. In Fig. 5(b), the average total volume of nanobubbles on each AFM image is calculated from Eq. (2). Our purpose of performing such a calculation is that the original sources of these gaseous interfacial nanobubbles are the gases (mainly  $\text{N}_2$ ,  $\text{O}_2$ ) dissolved in the cold water. Therefore, the total volume of interfacial nanobubbles on AFM image could be directly related to the excess gas dissolved in the cold water when it is warmed up at ambient temperature. In degassed and room temperature water, the total volume of nanobubbles is quiet small, consistent with the previous observations that nanobubbles rarely formed in the room temperature deionized water and degassed water.<sup>[56]</sup> Note that the heterogeneity of the substrate also affects the formation of nanobubbles, for example, nanobubbles tend to form near the steps of HOPG surface in many cases. This is why the error bars in Fig. 5 are quiet large. The total volume of nanobubbles increases with cooling time increasing and reaches a maximal value at the 48th hour. This means that

the amount of gas dissolved in the cold water is in equilibrium after cooling for more than 48 h. Therefore all the statistical results suggest that room temperature pure water cooled for more than 48 h at  $4^\circ\text{C}$  is sufficient enough to produce interfacial nanobubbles effectively on the HOPG surface.

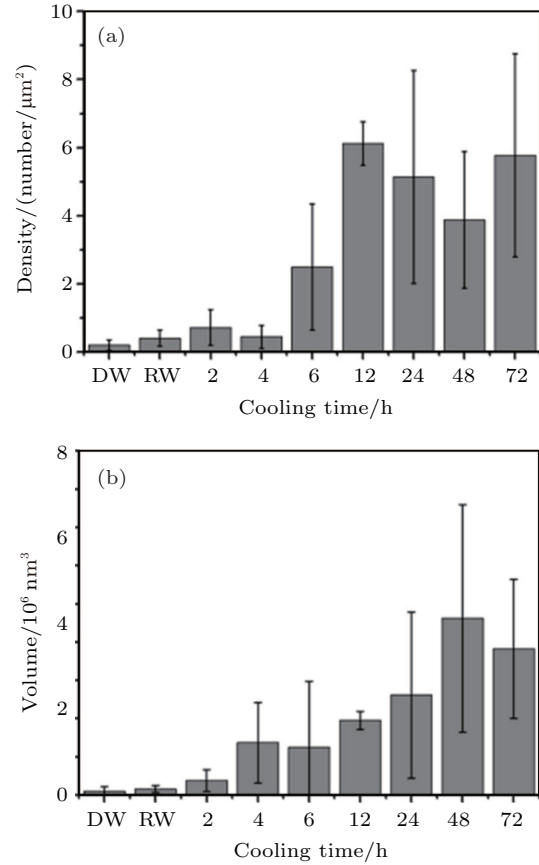


**Fig. 5.** Density and total volume of nanobubbles in the area produced by cold water with different cooling times, room temperature water and degassed water. Error bar is given by analyzing the AFM images scanned at different places on HOPG surface in the experiments. DW: degassed water, RW: room temperature water (0 h).

## 2.4. Effects of the dissolved gases on the nanobubble formation

In our method, the pure water is treated only by  $4^\circ\text{C}$  and the high temperature is avoided in all the processes. Our strategy is based on the fact that at lower temperature such as at  $4^\circ\text{C}$  the gas concentration would be higher than that at room temperature. Thus when the gas-saturated cold water is brought to the room temperature, an oversaturation state will be expected. This could be demonstrated by directly measuring the gas concentration in water.

Although most of the dissolved gases in water are nitrogen and oxygen, it is difficult to accurately measure the dissolved nitrogen in water. Alternatively, the dissolved oxygen is measured to understand how the excess dissolved gas affects the formation of nanobubbles in our method. As shown in Fig. 6 the concentrations and saturations of dissolved oxygen in cooled water increase when the cold water is cooled for longer hours. The dissolved oxygen increases to more than

10 mg/L (about 120% saturation) after cooling for 72 h. The concentration of dissolved oxygen in cold water is in equilibrium after cooling for more than 96 h. The concentration of equilibrium is about 11 mg/L.

While in the room temperature water (0 h), the dissolved gases are quite few (4.5 mg/L, 55% saturation) and no nanobubbles can be formed by such water. As shown in Fig. 5(b) with more dissolved gases in cold water, more nanobubbles are produced on the HOPG surface. Thus the total volume of interfacial nanobubbles is directly related to the volume of dissolved gases in cold water.

In the control experiments, room temperature water preserved at the room temperature over 72 h could not produce nanobubbles on HOPG. We further cool this gas-saturated water at room temperature in 4-°C refrigerator for half an hour and find very few nanobubbles on HOPG surface, either. This means that the cold pure water with saturated gas at room temperature is not sufficient to produce a lot of nanobubbles. All the experiments show that only the cold pure water with gas saturated (normally 100%–120% saturation) at 4 °C can achieve the high efficiency of nanobubbles production. The growth mechanism is simple and can be explained as follows. When the cold water on the HOPG surface is warmed up, the gases are in an oversaturated state. This can be seen from the measured gas saturation of the cold water cooled for over 72 h, which is 10 mg/L, about 120% oversaturated, as compared with the saturated concentration 8 mg/L at the room temperature. Then, a large quantity of the dissolved gases would release from the bulk water and aggregate onto the hydrophobic HOPG surface. Therefore nanobubbles could be easily formed with a high efficiency.

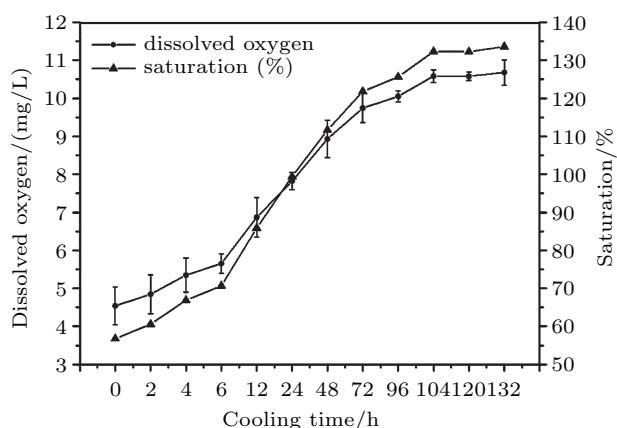


Fig. 6. Concentrations and saturations of the dissolved oxygen in cold water after different cooling times. The saturation rate is acquired by comparing with the 100% saturated water at 25 °C (8 mg/L).

### 3. Conclusions

In this work, we develop a contamination-free, one-step, and controllable method to effectively produce interfacial nanobubbles by cold water. The controlled experiments of degassing confirm that the spherical cap-shaped objects formed

on HOPG surface are indeed gaseous nanobubbles. The total quantity of nanobubbles formed on HOPG surface is found to be dominated by the concentration of dissolved gases in cold water. The dissolved oxygen measurement reveals that the gas saturation is a key factor to produce nanobubbles. The high efficiency of nanobubble nucleation can be achieved at high gas concentration. The density and size of formed nanobubbles can be controlled by different cooling times. Since only pure water is involved and the formation of nanobubbles is highly effective and convenient, this method may have its unique advantages for studying the properties of nanobubbles in a well-defined, contamination-free system and potential applications in nano-engineering, bio-molecule absorption and surface modification. Our results may also provide a new path to understand the effect of gas concentration on the evolution of interfacial nanobubbles.

## 4. Experiment

### 4.1. Materials

The highly oriented pyrolytic graphite (short as HOPG, 12 mm×12 mm, ZYB grade, Bruker) used as the substrate was freshly cleaved with double faced adhesive tape in each experiment. Deionized pure water (room temperature) was prepared with an ELGA PURELAB Classic water purification system to obtain a conductivity of 18.4 MΩ·cm. Degassed water was obtained by placing the water under 10 mbar for at least 2 h. The freeze-pump-thaw process (3 cycles) was also used to acquire fully degassed water. The glass beaker (50 mL, 18 mm in diameter) and glass syringe (5 mL) were pre-cleaned with chromic acid and clean water. The AFM liquid cell contains a translucent O-ring which was used to seal the fluid. Before each experiment these glass containers and AFM liquid cell were ultrasonic cleaned with ethanol (99.8%, GR) and then deionized pure water for 45 min separately and then dried at 70 °C for 1 min before being used. The cold water was injected to the fluid cell through Teflon inlet and outlet tube and silicone connectors. The Teflon tubes and connectors were ultrasonic cleaned with ethanol (99.8%, GR) and then deionized pure water and dried before usage.

### 4.2. Nanobubble formation

In order to produce interfacial nanobubbles, the deionized water was firstly preserved in a clean glass beaker and sealed with Parafilm (Laboratory Film, Parafilm Brand) while leaving several holes to contact the air environment, then the water was cooled in a 4-°C refrigerator for 2 h, 4 h, 6 h, 12 h, 24 h, 48 h, and 72 h. The Parafilm used to seal the glass beaker was a plastic paraffin film which is translucent, waterproof and odorless. Its potential effects on the purity of the water during the long term preservation were assessed in Appendix A (Fig. A1). The fresh cleaved HOPG surface at 25 °C

was placed inside the AFM liquid cell before the cooled water was injected. When being removed from refrigerator, the cold water was added to the HOPG surface immediately using a clean glass syringe. After the HOPG surface was immersed in the cold water for about 20 min–30 min, different areas of

the surface were imaged. The brief procedure was presented in Fig. 7. Each experiment was repeated at least 5 times independently and for each group at least 20 AFM images were collected for analysis.

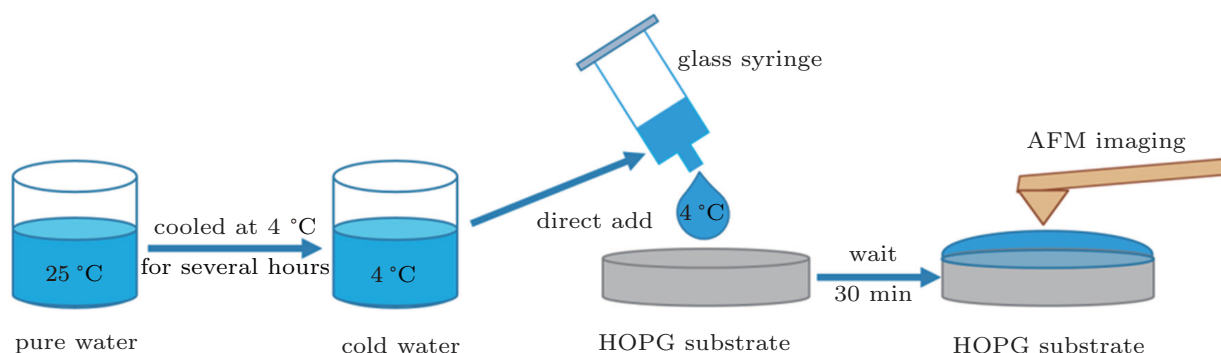


Fig. 7. (color online) A brief diagram of the procedure for the nanobubble production.

### 4.3. AFM experiments

PF-QNM (PeakForce Quantitative Nanomechanical Mapping) imaging in fluid was performed on a Bruker Multimode 8 SPM with NanoScope version 8.15 software and NanoScope V in order to quantitatively characterize the morphologies and stiffness of interfacial nanobubbles. The NPS-type probe (Bruker's silicon nitride probes with a nominal spring constant of 0.35 N/m and a tip radius of 10 nm) and SNL-type probe (Bruker's silicon nitride probes with a nominal spring constant of 0.1 N/m and a tip radius of 2 nm) were treated with a plasma cleaner (HARRICK PLASMA CLEANER PDC-32G) for about 3 min beforehand to achieve hydrophilicity and then immediately used to avoid being contaminated.

Following the standard PF-QNM imaging procedure, the deflection sensitivity and the spring constant of each cantilever were calibrated via PF-QNM ramp, thermal tuning on HOPG in water. The sample was oscillated vertically at a frequency of 2 kHz with an amplitude of 100 nm and a scan rate of 0.977 Hz. The Poisson ratio of the sample was set to be 0.5 as recommended by Multimode user guide to acquire reliable data while the stiffness of the sample was lower than 100 MPa. The peakforce set point was carefully selected and the loading force of imaging was about 200 pN–300 pN. Typical scan sizes were 5  $\mu\text{m}$  and scan time for each image was 4 min–5 min. All the PF-QNM imaging was performed under ambient condition at room temperature and the humidity was about 30%–50%.

Force volume imaging was performed at a resolution of 128 pixels  $\times$  128 pixels with a scan rate of 0.0254 Hz. The ramp sizes and trigger thresholds were set to be 100 nm and 18.25 nm. The tip approaching speed was set to be 1.3  $\mu\text{m}$ , and the number of points in a single approach–retraction cycle

was 512. The scan size was 5  $\mu\text{m}$  and for each image the scan took about 1 h. The force curves were presented as force versus separation, with the separation larger than 80 nm treated as the base line.

The offline AFM analysis program, NanoScope Analysis 1.5 was used for morphologies and mechanical property measurements and analyses. In particularly, particle analysis was performed to calculate the distribution and mean size of nanobubbles.

### 4.4. Dissolved oxygen measurement

The dissolved oxygen (DO) was measured by a dissolved oxygen meter (Orion Versa Star pro, VSTAR94, Thermo Scientific). The room temperature water was cooled at 4  $^{\circ}\text{C}$  for 2 h, 4 h, 6 h, 12 h, 24 h, 48 h, and 72 h before measurement. Because the temperature of the cold water would rise up very soon when removed from the 4- $^{\circ}\text{C}$  refrigerator, to avoid a possible deviation induced by temperature change, during the measurement the DO probe and the bottle of cold water were kept in an ice box to maintain a low temperature. Each measurement took about 2 min before the meter reached its equilibrium. The dissolved oxygen probe was calibrated in air-saturated water at 25  $^{\circ}\text{C}$ . The calibrated dissolved oxygen of air-saturated water at 25  $^{\circ}\text{C}$  was set to be 8 mg/L automatically by the meter. The experiments were repeated several times to acquire reliable data.

### Acknowledgement

We thank the staff of beamline 08U1A team at the Shanghai Synchrotron Radiation Facilities (SSRF) for the sample preparation and discussion.



Appendix A: Supporting information

To check whether the water purity has changed during the long term perseveration, the particles in deionized pure water and the same water persevered at 4 °C for 72 h are analyzed by dynamic light scattering using the Nanosight (NS300, Nanosight, Malvern, software Nanosight V3.2). The results show that the size of particles (normally 100 nm–200 nm) and its concentration ( $\sim 10^5/\text{mL}$ ) change little after being persevered at 4 °C for 72 h. This indicates that the long term perseveration does not change the purity of water, and at least does not introduce insoluble compounds into the cold water, either. The size distribution of particles in the cold water and deionized pure water is shown in Fig. A1.

The statistics data of nanobubbles produced by cold water cooled for 48 h at 4 °C are listed in Table A1. In the table each row represents the counted nanobubbles (numbers, mean

sizes, mean height, total volume, and coverage) in one AFM image.

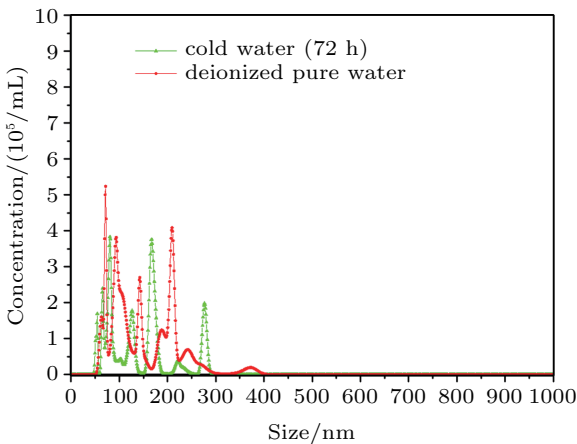


**Fig. A1.** (color online) Concentrations of particles with different sizes in deionized pure water (red circle) and cold water persevered at 4 °C for 72 h (green triangle). The data are obtained by dynamic light scattering measurement.

**Table A1.** statistics Data of nanobubbles produced by cold water cooled for 48 h at 4 °C.

Count for nanobubbles, area 5 $\mu\text{m} \times 5 \mu\text{m}$ , lateral size > 50 nm				
Numbers	Mean size/nm	Mean height/nm	Volume/ $\text{nm}^3$	Area/ $\mu\text{m}^2$
118	160.916	7.894	9502300.747	2.39977397
251	143.836	1.355	2763500.036	4.07848425
198	133.178	1.098	1514369.118	2.758163719
63	159.007	4.341	2718028.934	1.251016135
46	178.379	4.639	2668830.508	1.149569296
64	199.458	8.302	8320080.723	1.999736474
67	169.628	7.543	5725552.394	1.51411813
45	177.236	9.273	5166289.718	1.110212896
56	177.848	3.528	2455286.98	1.391156125
87	184.477	3.178	3696487.938	2.325378118
85	149.583	5.5	4115173.276	1.493734039
127	149.093	7.29	8107516.463	2.217216501
167	154.304	4.246	6636650.471	3.122918956
169	156.369	5.208	8463709.324	3.245472221
136	144.97	7.315	8238368.815	2.244838283
126	148.637	8.78	9642610.252	2.186322788
114	141.038	9.22	8257252.247	1.781012661
158	150.009	7.069	9899051.2	2.792425484
135	157.44	5.973	7864098.995	2.628172124
103	166.966	4.78	5395794.745	2.255190246
84	173.798	5.064	5051423.059	1.992777031
72	176.912	5.451	4829837.71	1.769852016
127	172.18	4.329	6405934.319	2.957052274
46	161.619	3.447	1627448.098	0.943696917
40	145.277	2.357	781673.8326	0.663045896
36	162.836	3.763	1411583.505	0.749709866
90	139.298	2.814	1930867.569	1.371583163
97	154.993	3.635	3328730.065	1.830146169
48	158.789	1.931	917930.589	0.950543374
55	163.278	1.425	820610.1416	1.151616577
67	148.289	2.959	1712884.281	1.157131056
66	170.384	1.98	1490063.63	1.504843819
55	167.375	1.682	1017860.389	1.210134781
Mean number	Mean size/nm		Mean volume/ $\text{nm}^3$	Mean area/ $\mu\text{m}^2$
96.90909091	160.5272727		4620539.396	1.88475895
50.05231423	14.49712962		2977539.155	0.797928053
Density/ $\mu\text{m}^2$				
3.876363636				
2.002092569				

## References

- [1] Parker J L Y V V and Claesson P M 1994 *J. Phys. Chem.* **98** 8468
- [2] Lou S T, Ouyang Z Q, Zhang Y, Li X J, Hu J, Li M Q and Yang F J 2000 *J. Vac. Sci. & Technol. B: Microelectronics and Nanometer Structures* **18** 2573
- [3] Ishida N, Inoue T, Miyahara M and Higashitani K 2000 *Langmuir* **16** 6377
- [4] Tyrrell J W and Attard P 2001 *Phys. Rev. Lett.* **87** 176104
- [5] Zhang L, Zhao B, Xue L, Guo Z, Dong Y, Fang H, Tai R and Hu J 2013 *J. Synchrotron Radiat.* **20** 413
- [6] Chan C U, Chen L, Arora M and Ohl C D 2015 *Phys. Rev. Lett.* **114** 114505
- [7] Hain N, Wesner D, Druzhinin S I and Schonherr H 2016 *Langmuir* **32** 11155
- [8] Granick S, Zhu Y and Lee H 2003 *Nat. Mater.* **2** 221
- [9] Wang Y and Bhushan B 2010 *Soft Matter* **6** 29
- [10] Pashley R M, Rzechowicz M, Pashley L R and Francis M J 2005 *J. Phys. Chem. B* **109** 1231
- [11] Thomas O C, Cavicchi R E and Tarlov M J 2003 *Langmuir* **19** 6168
- [12] Stöckelhuber K W, Radoev B, Wenger A and Schulze H J 2004 *Langmuir* **20** 164
- [13] Wu Z, Chen H, Dong Y, Mao H, Sun J, Chen S, Craig V S and Hu J 2008 *J. Colloid Interface Sci.* **328** 10
- [14] Liu G and Craig V S 2009 *ACS Appl. Mater. Interfaces* **1** 481
- [15] Gao L, Ni G X, Liu Y, Liu B, Castro Neto A H and Loh K P 2014 *Nature* **505** 190
- [16] Berkelaar R P, Zandvliet H J and Lohse D 2013 *Langmuir* **29** 11337
- [17] Wang L, Wang X, Wang L, Hu J, Wang C L, Zhao B, Zhang X, Tai R, He M, Chen L and Zhang L 2017 *Nanoscale* **9** 1078
- [18] Sobhy A and Tao D 2013 *Int. J. Miner. Process.* **124** 109
- [19] Liu Y and Dillon S J 2014 *Chem. Commun.* **50** 1761
- [20] An H, Liu G and Craig V S 2015 *Adv. Colloid Interface Sci.* **222** 9
- [21] Zhang X H, Khan A and Ducker W A 2007 *Phys. Rev. Lett.* **98** 136101
- [22] Borkent B M, Dammer S M, Schonherr H, Vancso G J and Lohse D 2007 *Phys. Rev. Lett.* **98** 204502
- [23] Brenner M P and Lohse D 2008 *Phys. Rev. Lett.* **101** 214505
- [24] Zhang L, Zhang X, Zhang Y, Hu J and Fang H 2010 *Soft Matter* **6** 4515
- [25] Seddon J R, Kooij E S, Poelsema B, Zandvliet H J and Lohse D 2011 *Phys. Rev. Lett.* **106** 056101
- [26] Craig V S J 2011 *Soft Matter* **7** 40
- [27] Seddon J R, Zandvliet H J and Lohse D 2011 *Phys. Rev. Lett.* **107** 116101
- [28] Weijss J H and Lohse D 2013 *Phys. Rev. Lett.* **110** 054501
- [29] Lohse D and Zhang X 2015 *Rev. Mod. Phys.* **87** 981
- [30] Plesset M S and Sadhal S S 1982 *Appl. Sci. Res.* **38** 133
- [31] Ducker W A 2009 *Langmuir* **25** 8907
- [32] Petsev N D, Shell M S and Leal L G 2013 *Phys. Rev. E* **88** 010402
- [33] Yasui K, Tuziuti T, Kanematsu W and Kato K 2015 *Phys. Rev. E* **91** 033008
- [34] Zhang L, Chen H, Li Z, Fang H and Hu J 2008 *Sci. China G: Phys. Mech. Astron.* **51** 219
- [35] Zhang X, Uddin M H, Yang H, Toikka G, Ducker W and Maeda N 2012 *Langmuir* **28** 10471
- [36] German S R, Wu X, An H, Craig V S, Mega T L and Zhang X 2014 *ACS Nano* **8** 6193
- [37] Xu C, Peng S, Qiao G G, Gutowski V, Lohse D and Zhang X 2014 *Soft Matter* **10** 7857
- [38] Berkelaar R P, Dietrich E, Kip G A, Kooij E S, Zandvliet H J and Lohse D 2014 *Soft Matter* **10** 4947
- [39] Lohse D and Zhang X 2015 *Phys. Rev. E* **91** 031003
- [40] Liu Y and Zhang X 2013 *J. Chem. Phys.* **138** 014706
- [41] Maheshwari S, van der Hoef M, Zhang X and Lohse D 2016 *Langmuir* **32** 11116
- [42] Liu Y and Zhang X 2014 *J. Chem. Phys.* **141** 134702
- [43] Zhang L J, Wang J, Luo Y, Fang H P and Hu J 2014 *Nucl. Sci. Tech.* **25** 060503
- [44] An H, Liu G, Atkin R and Craig V S 2015 *ACS Nano* **9** 7596
- [45] Shin D, Park J B, Kim Y J, Kim S J, Kang J H, Lee B, Cho S P, Hong B H and Novoselov K S 2015 *Nat. Commun.* **6** 6068
- [46] Lhuissier H, Lohse D and Zhang X 2014 *Soft Matter* **10** 942
- [47] Fang C K, Ko H C, Yang C W, Lu Y H and Hwang I S 2016 *Sci. Rep.* **6** 24651
- [48] Zhang X H, Zhang X D, Sun J L, Zhang Z X, Li G, Fang H P, Xiao X D, Zeng X C and Hu J 2007 *Langmuir* **23** 1778
- [49] Peng H, Hampton M A and Nguyen A V 2013 *Langmuir* **29** 6123
- [50] Lu Y H, Yang C W, Fang C K, Ko H C and Hwang I S 2014 *Sci. Rep.* **4** 7189
- [51] Zhang L, Zhang X, Fan C, Zhang Y and Hu J 2009 *Langmuir* **25** 8860
- [52] Li D, Pan Y, Zhao X and Bhushan B 2016 *Langmuir* **32** 11256
- [53] Li D, Jing D, Pan Y, Wang W and Zhao X 2014 *Langmuir* **30** 6079
- [54] Zargarzadeh L and Elliott J A 2016 *Langmuir* **32** 11309
- [55] Lou S T, Ouyang Z Q, Zhang Y, Li X J, Hu J, Li M Q and Yang F J 2000 *J. Vac. Sci. Technol. B* **18** 2573
- [56] Zhang X H, Zhang X D, Lou S T, Zhang Z X, Sun J L and Hu J 2004 *Langmuir* **20** 3813
- [57] Guo W, Shan H, Guan M, Gao L, Liu M and Dong Y 2012 *Surf. Sci.* **606** 1462
- [58] Zhang L, Zhang Y, Zhang X, Li Z, Shen G, Ye M, Fan C, Fang H and Hu J 2006 *Langmuir* **22** 8109
- [59] Guan M, Guo W, Gao L, Tang Y, Hu J and Dong Y 2012 *Chem. Phys. Chem.* **13** 2115
- [60] An H, Tan B H, Zeng Q and Ohl C D 2016 *Langmuir* **32** 11212
- [61] Wang L, Miao X and Pan G 2016 *Langmuir* **32** 11147
- [62] Zhao B, Song Y, Wang S, Dai B, Zhang L, Dong Y, Lü J and Hu J 2013 *Soft Matter* **9** 8837
- [63] Walczyk W and Schonherr H 2014 *Langmuir* **30** 7112
- [64] Wang Y, Wang H, Bi S and Guo B 2016 *Sci. Rep.* **6** 30021
- [65] Walczyk W, Hain N and Schonherr H 2014 *Soft Matter* **10** 5945
- [66] Guo Z, Liu Y, Xiao Q, Schonherr H and Zhang X 2016 *Langmuir* **32** 751
- [67] Wang X, Zhao B, Hu J, Wang S, Tai R, Gao X and Zhang L 2017 *Phys. Chem. Chem. Phys.* **19** 1108
- [68] An H, Tan B H and Ohl C D 2016 *Langmuir* **32** 12710
- [69] Zhang X H, Maeda N and Craig V S 2006 *Langmuir* **22** 5025